Supporting information

An electrochemically-induced bilayered structure facilitates long-life zinc storage of vanadium dioxide

Tongye Wei[1], Qian Li[1], Gongzheng Yang[1*], Chengxin Wang[1,2*]

[1]*State Key Laboratory of Optoelectronic Materials and Technologies, School of Materials Science and Engineering, Sun Yat-sen (Zhongshan) University, Guangzhou 510275, People's Republic of China*

[2]*The Key Laboratory of Low-carbon Chemistry & Energy Conservation of Guangdong Province, Sun Yat-sen (Zhongshan) University, Guangzhou 510275, People's Republic of China*

*Correspondence and requests for materials should be addressed to C. X. Wang.

Tel & Fax: +86-20-84113901

E-mail: wchengx@mail.sysu.edu.cn, ygongzh@mail2.sysu.edu.cn

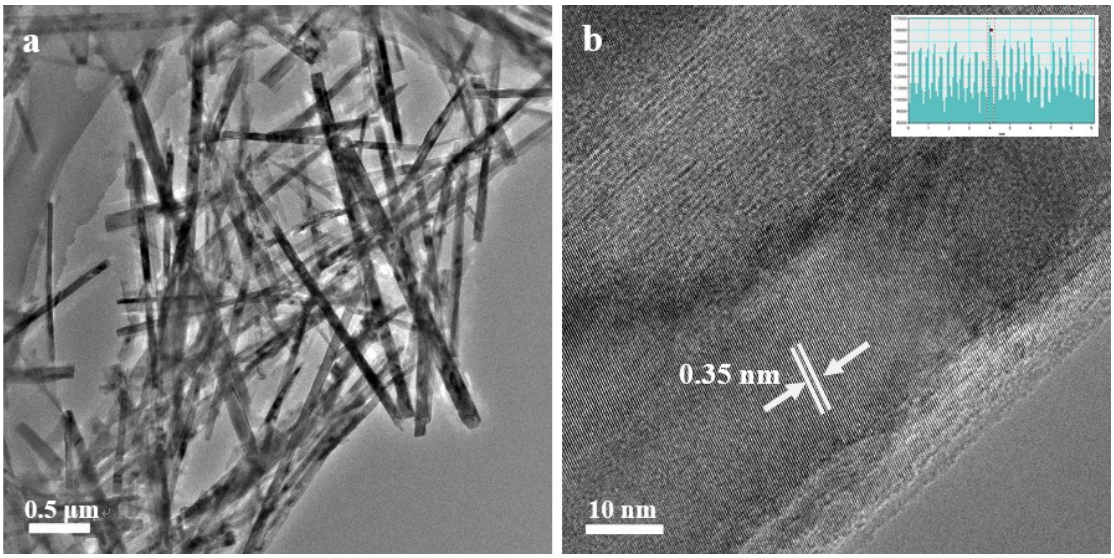

Figure S1. a) A panoramic TEM image of the prepared VO_2 nanobelts. b) A HRTEM image of an individual nanobelt shows its high crystallinity and the (110) lattice fringes with a *d*-spacing of 0.35 nm.

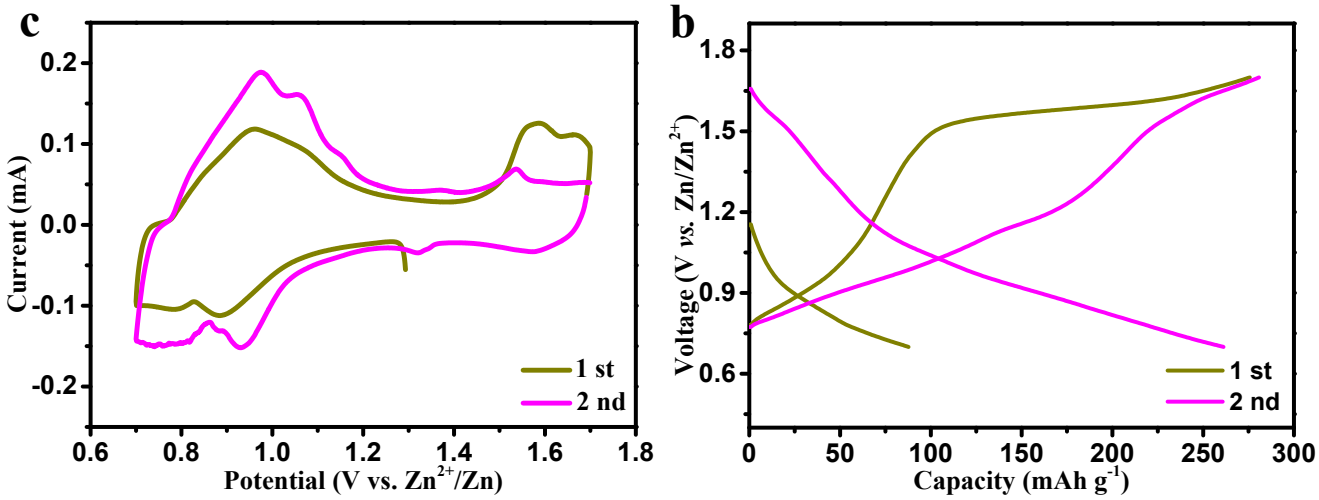

Figure S2. a) CV and b) charge-discharge curves of VO_2-based electrodes obtained in the first two cycles. The first discharge capacity is about 100 mAh g^{-1}. Upon charging process, an obvious plateau at 1.5 V is observed, where it is noticeable that the charge capacity at the end of 1.5 V is 100 mAh g^{-1}, suggesting the thorough extrusion of the Zn^{2+} ions from the electrode materials. Therefore, the oxidation peak (Figure S2a) at 1.5 – 1.7 V indicates an irreversible phase transition, which is in detailed discussed in the following morphological and structural analyses.

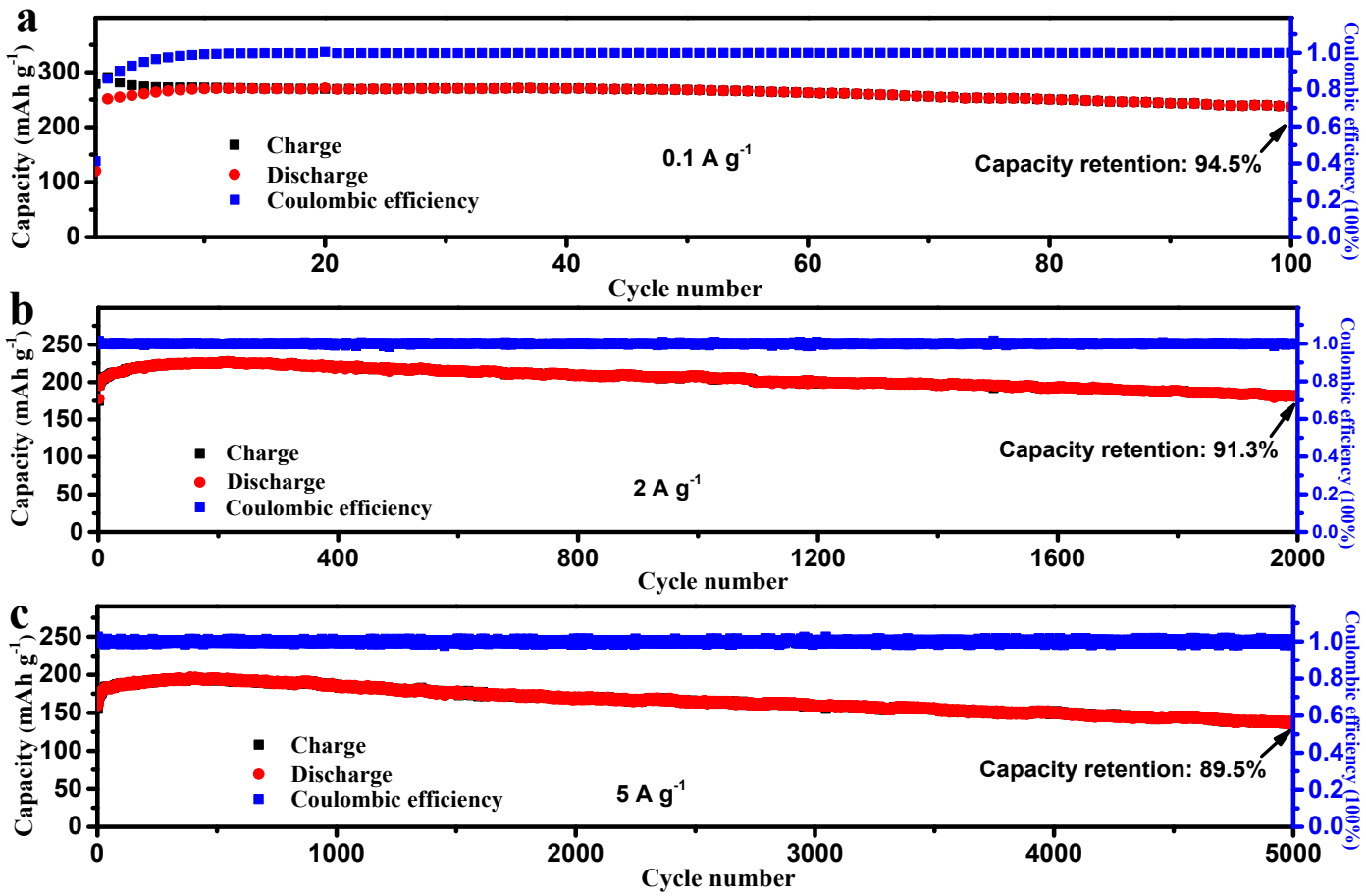

Figure S3. Long-term cycling performances of the VO_2/Zn Cell. Capacity as a function of cycle number obtained at the current densities of a) 0.1, b) 2, and c) 5 A g^{-1}.

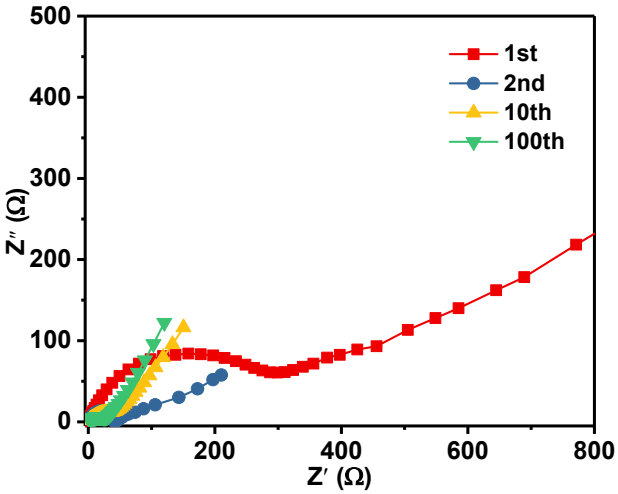

Figure S4. Nyquist plots of the VO_2 // Zn battery cell in the frequency range of 0.001–10000 Hz after different discharge-charge processes. The semicircle at high frequency range can be assigned to charge transfer progress, while an inclined line at low frequency region is ascribed to Zn^{2+} transfer in the host. Special attention is directed to charge transfer resistance (R_{ct}) which decreases sharply since the first cycle, indicating a significantly enhanced conductivity.

Table S1. Comparison of cycling properties of the VO_2 electrodes with reported cathode materials of rechargeable zinc ion batteries.

Samples	Specific capacity		Cycling performance			Ref.
	Current (mA g^{-1})	Capacity (mAh g^{-1})	Current (mA g^{-1})	Cycle number	Capacity retention	
VO_2	100	274.0	1000 10000	1000 10000	87% 79%	This work
BL-V_2O_5	14.4	170	14.4	120	89%	[1]
$Zn_{0.25}V_2O_5$	50	300	2.4	1000	81%	[2]
LiV_3O_8	16	256	133	65	75%	[3]
VS_2	50	190.3	500	200	98	[4]
$Na_3V_2(PO_4)_3$	50	97	50	100	74%	[5]
α–MnO_2	105	210	630	100	77%	[6]
α–MnO_2	102	285	1540	5000	92%	[7]
α–MnO_2	33	272	83	50	63%	[8]
α–MnO_2	16	270	73	75	43	[9]
α–MnO_2	10.5	195	42	30	70	[10]
Todorokite-type MnO_2	50	255	50	50	50%	[11]
MnO_2	110	210	1000	50	99%	[12]
γ-MnO_2	0.05	285	0.5	40	37%	[13]
δ-MnO_2	12.3	123	12.3	100	57%	[14]
δ-MnO_2	83	252	83	100	50%	[15]
Mn_2O_3	100	141	100	30	87%	[16]
$Na_{0.44}MnO_2$	24	186.2	480	100	40%	[17]
Spinel $ZnMn_2O_4$	50	150	500	500	94%	[18]
$LiNi_{1/3}Co_{1/3}Mn_{1/3}O_2$	50	115	20	40	99%	[19]
$K_{0.86}Ni[Fe(CN)_6]_{0.954}(H_2O)_{0.76}$	11.2	55.6	11.2	36	91%	[20]
Zinc hexacyanoferrate	60	69.1	300	100	93%	[21]
Zinc Hexacyanoferrate	60	65.4	60	100	81%	[22]
Copper hexacyanoferrate	20	56	20	20	77%	[23]
Copper hexacyanoferrate	60	61	300	500	83%	[24]

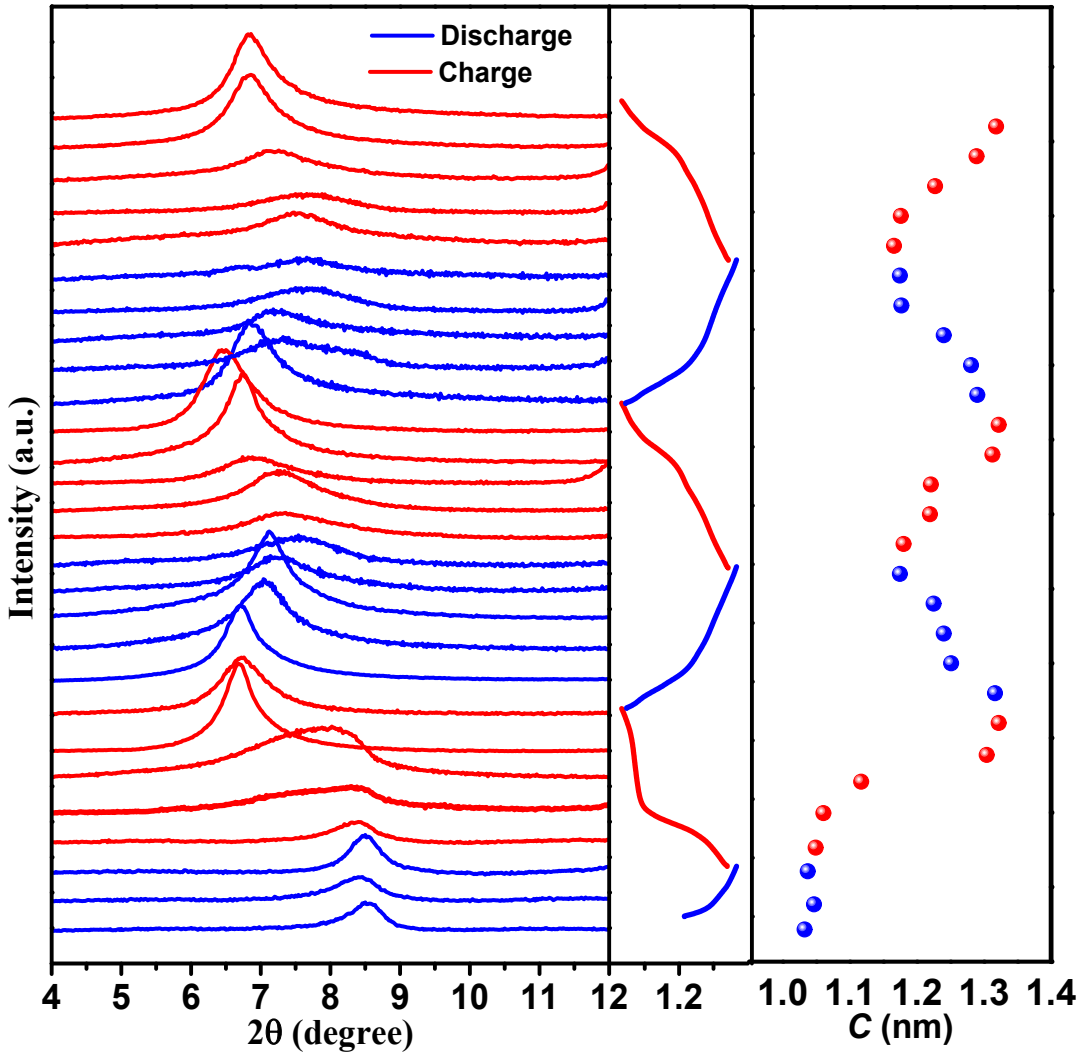

Figure S5. Electrochemical mechanism study of the VO_2 cathode material: (001) diffraction peak of the XRD patterns at different states (Left); discharge-charge profiles in the first three cycles (Middle); changes of the lattice parameter calculated according to the (001) diffraction peak (Right). Close observations reveal that the lattice parameter increasing rapidly during charging process at *ca.* 1.4 V in the first cycle, as illustrated by a sharp shift in (001) diffraction peak to smaller angels. Thereafter the *d*-spacing demonstrates a periodic fluctuation, suggesting the stable structure upon zinc-based cations intake/removal.

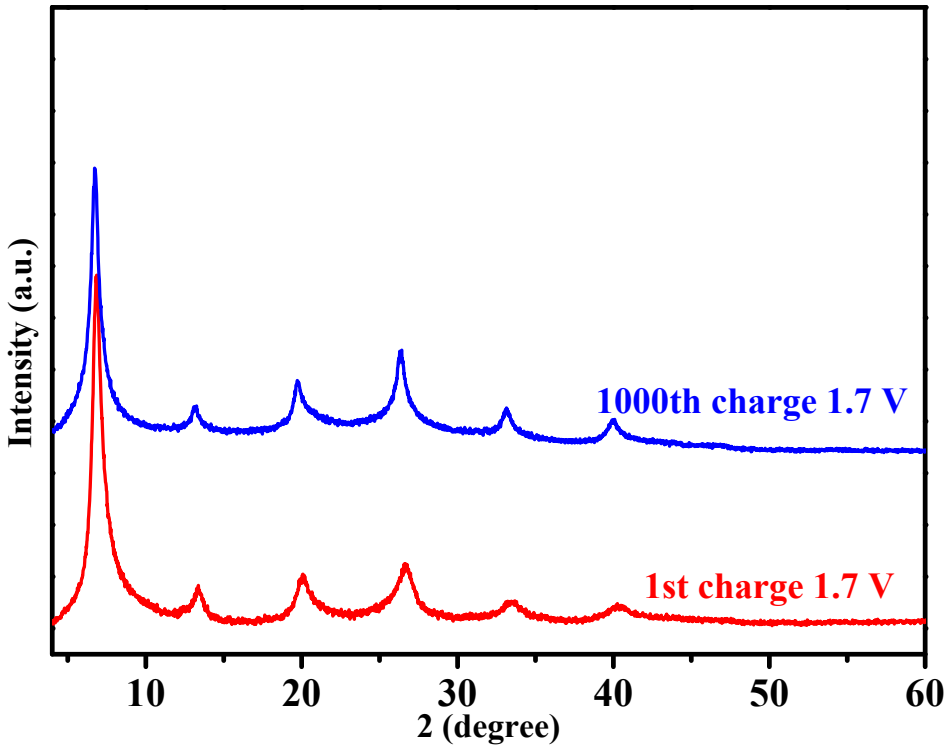

Figure S6. XRD patterns of VO_2 cathodes charged to 1.7 V at the first and after 1000 cycles.

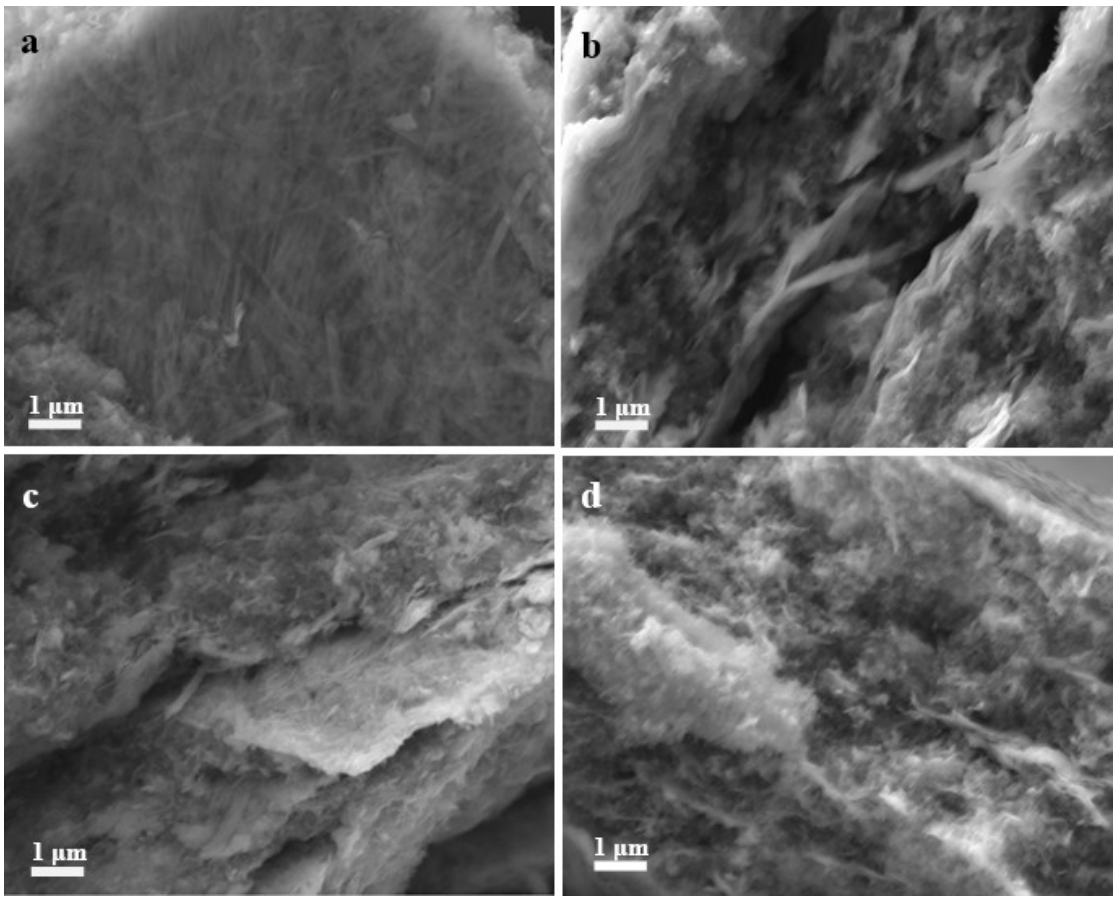

Figure S7. SEM images of the VO_2 electrodes at different stage. a) SEM image of the electrode discharged to 0.7 V in the first cycle, in which nanobelts are clearly observed. b) SEM image of the electrode charged to 1.7 V in the first cycle. Interestingly, nearly all the nanobelts have transformed to nanosheets during the charging process. c) SEM image of the electrodes discharged to 0.7 V and d) SEM image of the electrodes charged to 1.7 V in the second cycle. The sheet-like morphologies are maintained since the first charging process.

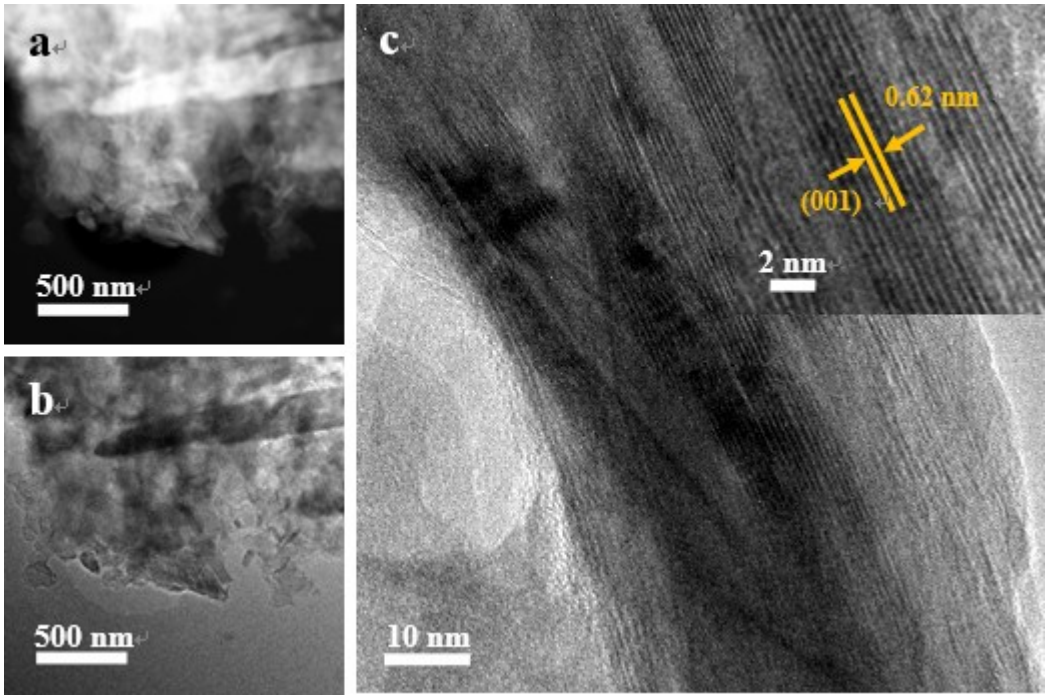

Figure S8. a) STEM, b) TEM, and c) HRTEM images of the VO_2 electrodes obtained as discharged to 0.7 V in the initial cycle. We can see that most of the electrodes still demonstrate the belt-like morphology, while HRTEM image (inset in c) presents a regular spacing of 0.62 nm that corresponds to the d_{001} spacing of VO_2, indicating that the phase has not changed in the first discharging process.

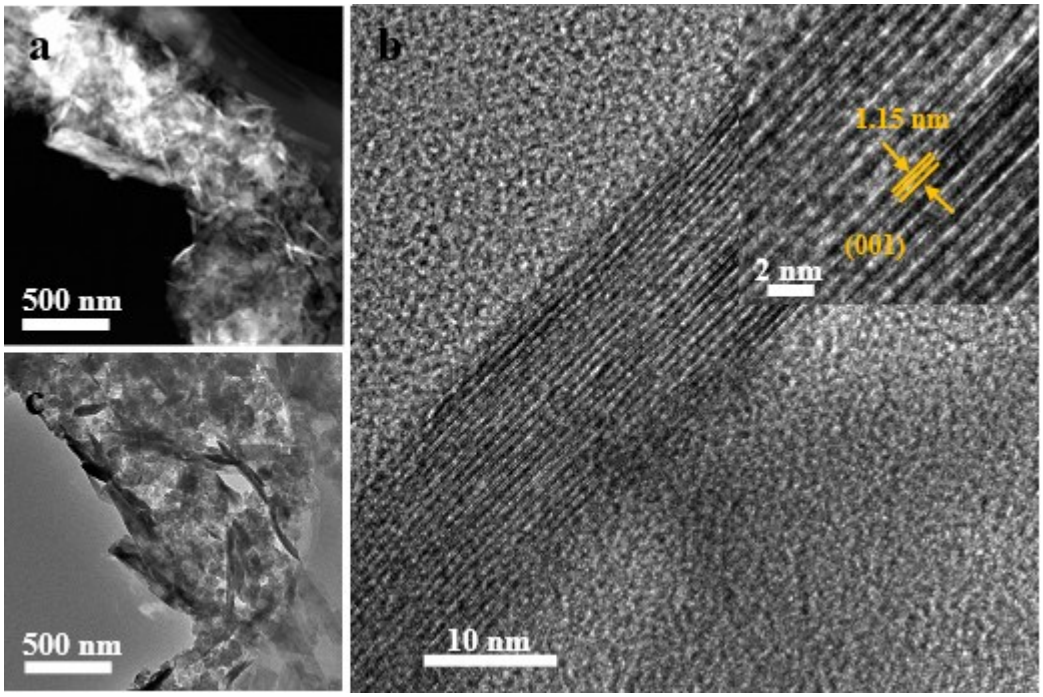

Figure S9. a) STEM, b) TEM, and c) HRTEM images of the VO_2 electrodes obtained as charged to 1.4 V in the initial cycle. We can see that the electrodes are composed of belt- and sheet-like morphologies. A HRTEM image (inset in c) exhibits a bilayer spacing of 1.15 nm, indicating that the phase has gradually changed in the current stage.

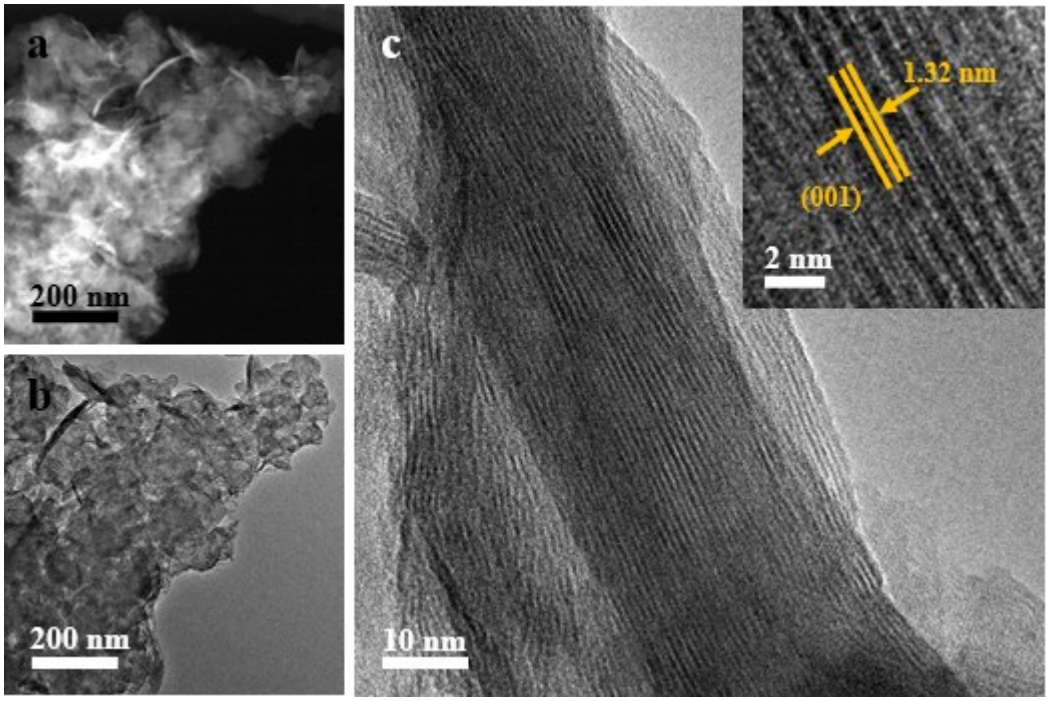

Figure S10. a) STEM, b) TEM, and c) HRTEM images of the VO_2 electrodes obtained as charged to 1.7 V in the initial cycle. We can see that almost all the electrodes demonstrate the sheet-like morphology, while HRTEM image (inset in c) presents a bilayer spacing of 1.32 nm that corresponds to the d_{001} spacing of $V_2O_5 \cdot nH_2O$, indicating that the phase has completely changed after the first charging process.

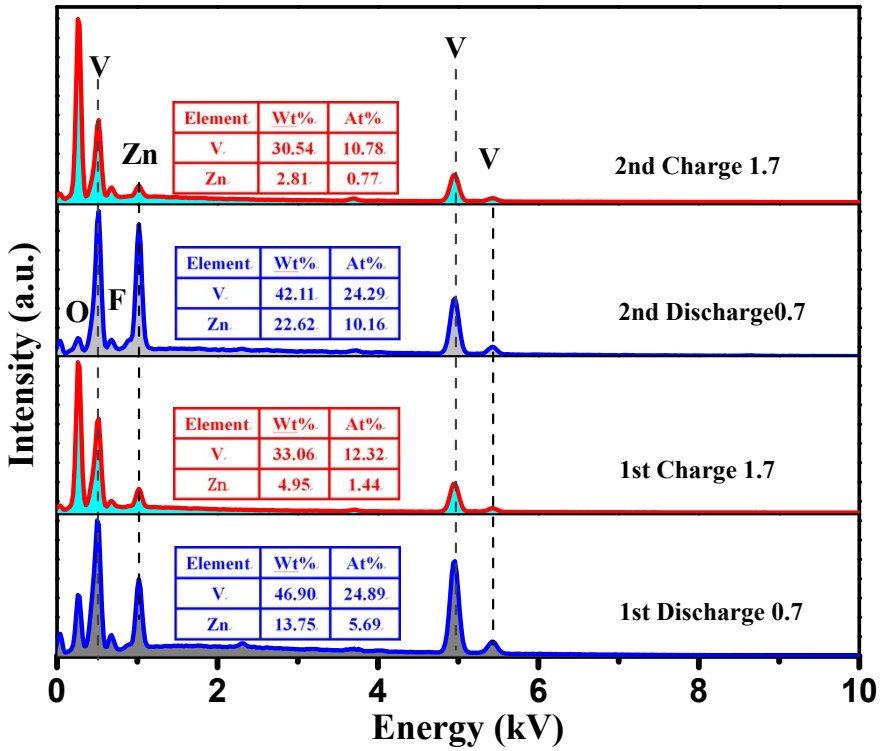

Figure S11. Energy dispersive X-ray spectra of the VO_2 electrodes collected at fully discharge/charge states in the first two cycles. Of particular note is the Zn content in the second discharge process nearly twice that of the first cycle, which agrees well with the galvanostatic charge/discharge results.

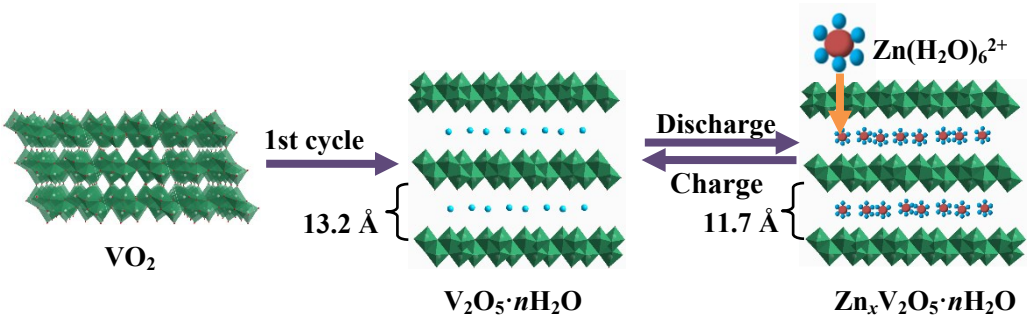

Figure S12. Schematic illustration of the phase transition of VO_2 cathode during cycling.

The SEM and TEM images of electrode obtained when discharge to 0.7 V are depicted in Figure S7a and Figure S8, which reveal that the nanobelt maintain well after the first cycle. A HRTEM image (inset in Figure 7c) presents a regular spacing of 0.62 nm that corresponds to the d_{001} spacing of VO_2, indicating that the phase has not changed in the first discharging process. As charging to the 1.4 V, the HRTEM image (inset in Figure S8c) exhibits a bilayer spacing of 1.15 nm, while both the sheet-like and belt-like morphology can be observed in the Figure S8a and b that means that the phase and morphology evolutions start at 1.4 V. With continue charging to 1.7 V, from Figure S7b and Figure S10, we can only observe sheet-like morphology. Moreover, a bilayer spacing of 1.32 nm that corresponds to the d_{001} spacing of $V_2O_5{\cdot}nH_2O$ was observed in Figure S10c, verifying that the VO_2 have been electrochemically-induced to bilayered structure $V_2O_5{\cdot}nH_2O$. Furthermore, the Zn contents of the electrode at different stages are investigated by the EDS, which demonstrate the Zn^{2+} insertion and extraction in the cathode material at different stages. Combining with the XRD patterns (Figure 4a) the phase transition of VO_2 can be illustrated as Figure S12. In the initial charge/discharge cycle, the cathode materials occur an irreversible transformation from the belt-like VO_2 to sheet-like $V_2O_5{\cdot}nH_2O$. The bilayered $V_2O_5{\cdot}nH_2O$ illustrates more stable and high electrochemical activity, which can reversibly accommodate Zn^{2+} insertion/extraction during the following discharge/charge processes.

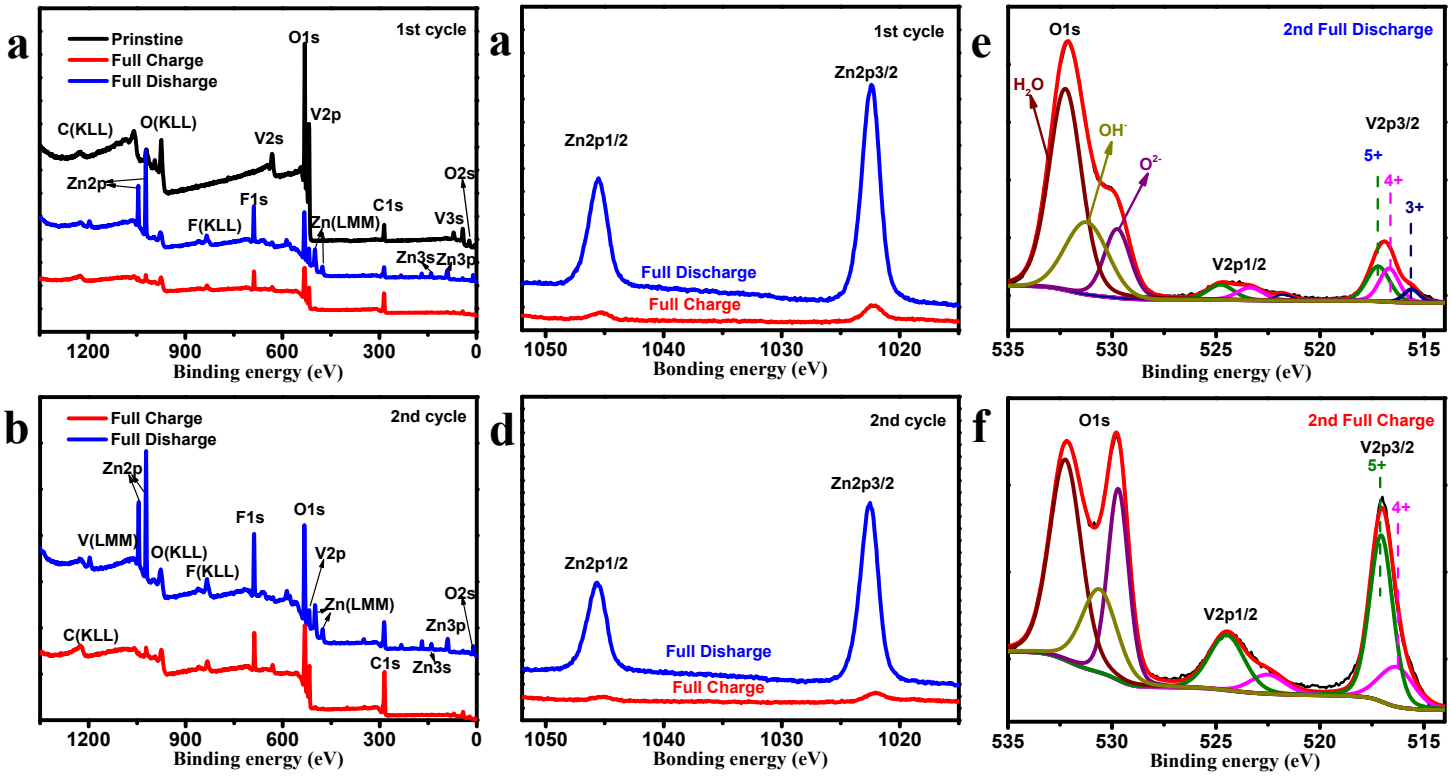

Figure S13. XPS spectra of the VO_2 electrodes. a, b) Survey spectra, c, d) Zn 2*p* region obtained at first and second cycle. e, f) V 2*p* and O 1*s* region of the XPS spectra in the second cycle.

References

1 P. Senguttuvan, S.-D. Han, S. Kim, A. L. Lipson, S. Tepavcevic, T. T. Fister, I. D. Bloom, A. K. Burrell and C. S. Johnson, *Adv. Energy Mater.,* 2016, **6**, 1600826.

2 D. Kundu, B. D. Adams, V. Duffort, S. H. Vajargah and L. F. Nazar, *Nat. Energy,* 2016, **1**, 16119.

3 M. H. Alfaruqi, V. Mathew, J. Song, S. Kim, S. Islam, D. T. Pham, J. Jo, S. Kim, J. P. Baboo, Z. Xiu, K.-S. Lee, Y.-K. Sun and J. Kim, *Chem. Mater.,* 2017, **29**, 1684–1694..

4 P. He, M. Yan, G. Zhang, R. Sun, L. Chen, Q. An and L. Mai, *Adv. Energy Mater.,* 2017,1601920.

5 G. L. Li, Z. Yang, Y. Jiang, C. H. Jin, W. Huang, X. L. Ding and Y. H. Huang, *Nano Energy,* 2016, **25**, 211–217.

6 C. J. Xu, B. H. Li, H. D. Du and F. Y. Kang, *Angew.Chem., Int. Ed.* 2012, **51**, 933–935.

7 H. Pan, Y. Shao, P. Yan, Y. Cheng, K. S. Han, Z. Nie, C. Wang, J. Yang, X. Li, P. Bhattacharya, K. T. Mueller and J. Liu, *Nat. Energy,* 2016, **1**, 16039.

8 M. H. Alfaruqi, J. Gim, S. Kim, J. Song, J. Jo, S. Kim, V. Mathew and J. Kim, *J. Power Sources,* 2015, **288**, 320–327.

9 M. H. Alfaruqi, S. Islam, J. Gim, J. Song, S. Kim, D. T. Pham, J. Jo, Z. Xiu, V. Mathew and J. Kim, *Chem. Phy. Lett.,* 2016, **650**, 64-68.

10 B. Lee, H. R. Lee, H. Kim, K. Y. Chung, B. W. Cho and S. H. Oh, *Chem. Commun.,* 2015, **51**, 9265–9268.

11 J. Lee, J. B. Ju, W. I. Cho, B. W. Cho and S. H. Oh, *Electrochim. Acta,* 2013, **112**, 138–143.

12 C. Xu, H. Du, B. Li, F. Kang and Y. Zeng, *Electrochem. Solid-State Lett.,* 2009, **12**, A61.

13 M. H. Alfaruqi, V. Mathew, J. Gim, S. Kim, J. Song, J. P. Baboo, S. H. Choi and J. Kim, *Chem. .Mater.,* 2015, **27**, 3609–3620.

14 S.-D. Han, S. Kim, D. Li, V. Petkov, H. D. Yoo, P. J. Phillips, H. Wang, J. J. Kim,

K. L. More, B. Key, R. F. Klie, J. Cabana, V. R. Stamenkovic, T. T. Fister, N. M. Markovic, A. K. Burrell, S. Tepavcevic and J. T. Vaughey, *Chem.Mater.,* 2017, **29**, 4874–4884.

15 M. H. Alfaruqi, J. Gim, S. Kim, J. Song, D. T. Pham, J. Jo, Z. Xiu, V. Mathew and J. Kim, *Electrochem. Commun.,* 2015, **60**, 121–125.

16 B. Jiang, C. Xu, C. Wu, L. Dong, J. Li and F. Kang, *Electrochim.Acta* 2017, **229,** 422–428.

17 X. Wu, Y. Li, Y. Xiang, Z. Liu, Z. He, X. Wu, Y. Li, L. Xiong, C. Li and J. Chen, *J.Power Sources,* 2016, **336**, 35–39.

18 N. Zhang, F. Cheng, Y. Liu, Q. Zhao, K. Lei, C. Chen, X. Liu and J. Chen, *J. Am. Chem. Soc.,* 2016, **138**, 12894–12901.

19 F. Wang, Y. Liu, X. Wang, Z. Chang, Y. Wu and R. Holze, *ChemElectroChem,* 2015, **2**, 1024–1030.

20 M. S. Chae, J. W. Heo, H. H. Kwak, H. Lee and S.-T. Hong, *J. Power Sources,* 2016, **337**, 204–211.

21 L. Y. Zhang, L. Chen, X. F. Zhou and Z. P. Liu, *Sci. Rep.***2015**, 5.

22 L. Zhang, L. Chen, X. Zhou and Z. Liu, *Adv. Energy Mater.,* 2015, **5**, 1400930.

23 Z. J. Jia, B. G. Wang and Y. Wang, *Mate. Chem. Phy.,* 2015, **149**, 601–606.

24 T. Gupta, A. Kim, S. Phadke, S. Biswas, T. Luong, B. J. Hertzberg, M. Chamoun, K. Evans-Lutterodt and D. A. Steingart, *J.Power Sources,* 2016, **305**, 22–29.